

Neutron-powder-diffraction study of $\text{YFe}_{12-x}\text{Mo}_x$ and $\text{YFe}_{12-x}\text{Mo}_x\text{N}_{1.0}$ ($x = 1$ and 3)

Hong Sun

Faculty of Integrated Arts and Sciences, Hiroshima University, Higashi-hiroshima 724, Japan

Y. Morii

Department of Physics, Japan Atomic Energy Research Institute, Tokai, Ibaraki 319-11, Japan

H. Fujii and M. Akayama

Faculty of Integrated Arts and Sciences, Hiroshima University, Higashi-hiroshima 724, Japan

S. Funahashi

Department of Physics, Japan Atomic Energy Research Institute, Tokai, Ibaraki 319-11, Japan

(Received 3 May 1993)

$\text{YFe}_{12-x}\text{Mo}_x$ ($x=1$ and 3) and full-charged nitrides were prepared. Neutron-powder-diffraction experiments were performed at 10 K and room temperature on both the host compounds and their nitrides. The Rietveld technique was used for data analysis. Mo was found to reside mainly on the $8i$ site in the tetragonal ThMn_{12} structure (space group $I4/mmm$), with a small fraction on the $8f$ site. The nitrides retain the crystallographic symmetry of the host compounds. Nitrogen atoms are located on the $2b$ site with nearly 100% occupancy. The nitrogenation-induced modification of the rare-earth environment and in turn the magnetocrystalline anisotropy properties are discussed. The refined moments are comparable with those obtained by magnetization measurement.

I. INTRODUCTION

Interstitially modified intermetallic materials based on rare-earth (R) atoms and iron have been studied quite intensively in recent years, especially since the work by Coey and Sun on nitrogenated $R_2\text{Fe}_{17}$ in early 1990.¹ Attention has been mainly focused on compounds with the 2:17 ($\text{Th}_2\text{Zn}_{17}$ and $\text{Th}_2\text{Ni}_{17}$ type) and 1:12 (ThMn_{12} type) structures where H, C, and N were used as interstitial atoms, although there are a few reports on other structure-type materials, such as $\text{Nd}_2\text{Fe}_{14}\text{B}$ (Ref. 2) and 1:5 (Ref. 3) compounds or using other elements as interstitials, B, for example.⁴ A brief review in this field was given by Wallace and Huang.⁵ In general, the magnetic properties of intermetallic compounds are very sensitive to the presence of interstitial atoms.⁶ After introducing interstitial nitrogen atoms into the crystallographic lattices, Curie temperature (T_c) was found to be increased by about 400 K on average over the rare-earth series in $R_2\text{Fe}_{17}$ (Ref. 7) and by about 200 K in $R\text{Fe}_{11}\text{Ti}$ series.⁸ In addition, the crystal-field environment of rare-earth atoms was also significantly modified, resulting in a strong uniaxial easy-magnetization direction at room temperature for $\text{Sm}_2\text{Fe}_{17}\text{Z}_y$ (Ref. 9) and $\text{NdFe}_{11}\text{TiZ}_y$ (Ref. 10) ($Z=\text{N}$ and C). As their intrinsic magnetic properties are comparable with those of $\text{Nd}_2\text{Fe}_{14}\text{B}$, they are promising candidates for permanent magnet applications. Actually, efforts towards coercivity development started immediately after the announcement of the formation of $R_2\text{Fe}_{17}\text{N}_{3-\delta}$ by gas-phase interstitial modification process.¹ Coercivity field as high as 4.4 T at room temperature (RT) was obtained on $\text{Sm}_2\text{Fe}_{17}\text{N}_{3-\delta}$ using mechanical alloying and metallic bonding methods together.¹¹

In order to understand physically the influences of interstitials on the magnetic properties, it is imperative to investigate the role that the interstitials played on the microscopic scale, particularly the crystallographic sites occupied by the interstitial atoms. Neutron-scattering experiments, which is a useful method for solving this problem, have been carried out by a number of research groups on both 2:17 and 1:12 nitrides.¹² While definitive conclusions have been drawn on the 2:17 nitrides, such as work by Isnard *et al.* on $\text{Pr}_2\text{Fe}_{17}$ and $\text{Pr}_2\text{Fe}_{17}\text{N}_{2.9}$,¹³ data and analyses on the 1:12 nitrides are not very satisfactory up to our knowledge. Problems mainly arise from that the sample quality is not perfect, resulting in a severe broadening of the diffraction peaks and in turn reducing the reliability of the results significantly.

In our previous work, we studied the intrinsic magnetic properties of $\text{YFe}_{12-x}\text{Mo}_x$ ($0.5 \leq x \leq 4.0$) series and their nitrides.¹⁴ Judging by the very well-defined x-ray-diffraction peaks and sharp magnetic phase transitions at Curie temperature, we believe our 1:12 Mo nitrides are the best among all the 1:12 nitrides. Here we report our neutron-powder-diffraction study on two of the members in the series, $x=1$, and 3 , both the host compounds and their corresponding nitrides. Apart from determining the interstitial N position, we also investigated in detail the preference occupation of Mo among the three different Fe sites.

II. EXPERIMENTAL DETAILS

A. Sample preparation

Sample preparations are similar to those described in Ref. 14, except a much bigger amount of samples was re-

quested by neutron-diffraction experiments. Ingots of YFe_{11}Mo and YFe_9Mo_3 were synthesized by arc-melting in 0.1 MPa flowing-argon atmosphere. The starting materials were of at least 99.9% purity. Each ingot was remelted several times to ensure homogeneity. The as-melted ingots were wrapped by tantalum foil, sealed in evacuated quartz tubes, annealed at 1373 K for 3 days, and then quenched into water.

The annealed ingots were ground into powder with particle size less than 20 μm in diameter. Nitrogenation was performed by heating the powder at 773 K for 12 h under 6 MPa high-purity (99.9999%) nitrogen gas. The amount of nitrogen uptake, which was determined by sample mass increase upon nitrogenation, yields a value of 1.0 ± 0.1 N atoms per formula unit for YFe_{11}Mo and 1.4 ± 0.1 for YFe_9Mo_3 . Owing to the relative large amount of sample produced each time (~ 3 g), the mass increase could be quite accurately measured.

Both standard powder x-ray diffraction (XRD) with $\text{Cu-K}\alpha$ radiation and thermal magnetic analysis (TMA) were used for checking the quality of samples. While YFe_{11}Mo was of single phase before nitrogenation, a small amount of Fe-Mo impurities is observable in YFe_9Mo_3 . Traces of iron appeared in both the samples after nitrogenation. Sharp magnetic phase transition at T_C revealed by TMA curves confirmed that the samples were mainly of single phase and the nitrogenation was homogeneous. For details of XRD and TMA results, see Ref. 14.

Inspecting the sample preparation procedures reported so far, the basic feature in our method is the high N_2 gas pressure (6 MPa), while other research groups used gas pressure in the order of 0.1 MPa (atmosphere pressure). This difference could be the reason that the quality of our sample is much better. The nitrogenation apparatus in Hiroshima University allows one to use gas pressure up to 10 MPa, which provides further advantages compared with only normal pressure.^{15,16}

B. Neutron-powder-diffraction experiments and data analysis

Neutron-diffraction experiments were carried out at the JRR-3M High Resolution Neutron Powder Diffractometer (HRPD) of Japan Atomic Energy Research Institute. The HRPD is an ILL-D2B-type diffractometer with 64 detector systems placed at every 2.5 degree of diffraction angle.¹⁷ The sample was contained in a 10 mm diameter and 30 mm height vanadium can. All the data were taken at $\lambda = 1.823$ Å (from a Ge 331 monochromator) and were collected for about 24 h in the 2θ range from 5° to 165° with step size 0.05° . Intensity data from $2\theta = 5^\circ$ to 155° were used in the refinements. YFe_{11}Mo and $\text{YFe}_{11}\text{MoN}_{1.0}$ were measured at both RT and 10 K, while YFe_9Mo_3 and $\text{YFe}_9\text{Mo}_3\text{N}_{1.0}$ were measured at RT only.

The diffraction data were analyzed using RIETAN, which was developed for the application of the Rietveld method to angle-dispersive x-ray and neutron-powder data.¹⁸ RIETAN can deal with mixtures of two or more phases, as well as can handle magnetic structures with collinear spin arrangements. The neutron-scattering

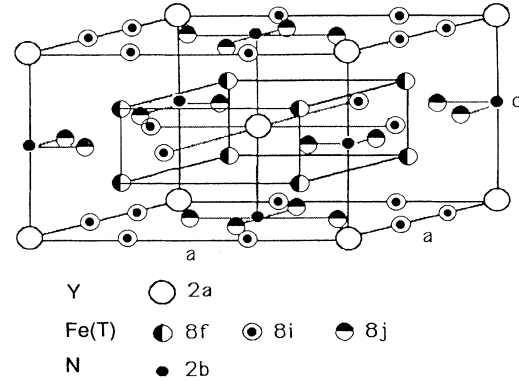


FIG. 1. Schematic diagram of the unit cell of the ThMn_{12} -type structure.

lengths used during the refinement of the structure were $b_Y = 7.750$, $b_{\text{Fe}} = 9.540$, $b_{\text{Mo}} = 6.950$, and $b_N = 9.360$ in units of 10^{-15} m.¹⁹ Magnetic form factors were taken from Ref. 20. The quality of the fits between the observed and calculated patterns was indicated by the reliability factors R_I and R_F , with,

$$R_I = \frac{\sum_k |I_k(o) - I_k(c)|}{\sum_k I_k(o)},$$

$$R_F = \frac{\sum_k |\sqrt{I_k(o)} - \sqrt{I_k(c)}|}{\sum_k \sqrt{I_k(o)}},$$

where $I_k(o)$ is the integrated intensity evaluated from summation of contributions of the k th peak to net observed intensities and $I_k(c)$ is the integrated intensity calculated from refined parameters.

TABLE I. Refined parameters of YFe_{11}Mo and $\text{YFe}_{11}\text{MoN}_{1.0}$ at room temperature. n is the occupation factor; x , y , and z are the fractional coordinate; B is the isotropic thermal parameter (\AA^2); and m is the magnetic moment (μ_B/atom). Numbers in parentheses are the *statistical* error given by the refinement program.

YFe ₁₁ Mo: $R_I = 6.38\%$; $R_F = 4.68\%$							
Site	Atom	n	x	y	z	B	m
2a	Y	1.0	0	0	0	0.45	0
8i	Fe	0.80(2)	0.358(1)	0	0	0.24	1.50(54)
	Mo	0.20(2)	0.358(1)	0	0	3.25	0
8j	Fe	1.00(2)	0.276 9(9)	0.5	0	0.24	1.50(54)
8f	Fe	0.95(2)	0.25	0.25	0.25	0.24	1.50(54)
	Mo	0.05(2)	0.25	0.25	0.25	3.25	0
YFe ₁₁ MoN _{1.0} : $R_I = 3.64\%$; $R_F = 2.97\%$							
2a	Y	1.0	0	0	0	1.0	0
8i	Fe	0.80(2)	0.360 6(9)	0	0	0.36	1.65(35)
	Mo	0.20(2)	0.360 6(9)	0	0	3.06	0
8j	Fe	1.00(2)	0.276 3(8)	0.5	0	0.36	1.65(35)
8f	Fe	0.95(2)	0.25	0.25	0.25	0.36	1.65(35)
	Mo	0.05(2)	0.25	0.25	0.25	3.06	0
2b	N	0.96(8)	0	0	0.5	0.49	0

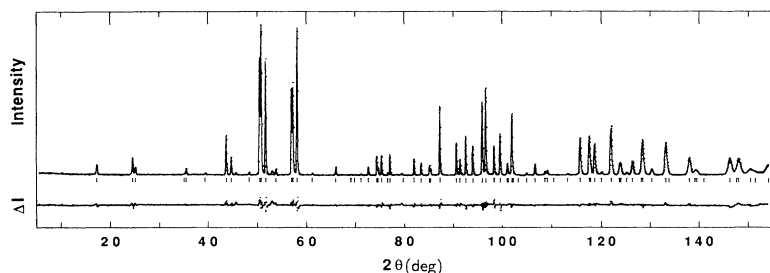


FIG. 2. Neutron-powder-diffraction pattern of YFe_{11}Mo at 10 K. The dots and line correspond to the observed and the calculated patterns, respectively. The lower part is the difference pattern (observed-calculated). The calculated peak positions are indicated by the bars.

III. RESULTS AND DISCUSSION

A. YFe_{11}Mo

It has been well established that compounds with the formula $\text{YFe}_{12-x}\text{T}_x$ ($T=\text{Ti}$, V , and Mo , etc.) crystallize in the tetragonal ThMn_{12} -type structure (body-centered tetragonal (bct), space group I4/mmm , No. 139). As shown in Fig. 1, there is one single crystallographic site ($2a$) occupied by Y and there are three different sites ($8i$, $8j$, and $8f$) occupied by Fe and T metals. We fitted the diffraction patterns of YFe_{11}Mo by using the same structure as the starting model. The diffraction pattern of YFe_{11}Mo at 10 K is shown in Fig. 2. Refinement results are summarized in Tables I and II for data at RT and 10 K, respectively. Interatomic distances at 10 K are listed in Table IV, refined parameters for YFe_9Mo_3 and $\text{YFe}_9\text{Mo}_3\text{N}_{1.0}$ are in Table III, and the lattice parameters are included in Table V.

During the refinements, special attention was paid to the occupation factor of Mo at different Fe sites. The best fit was given by occupying 20% of the $8i$ site and 5% of the $8f$ site. The preferred occupation of T elements among the three Fe sites in $\text{YFe}_{12-x}\text{T}_x$ has been discussed in terms of the size of T atoms, the crystallographic environment of the particular Fe site, and the heat of

formation between T atoms and rare-earth atoms.²¹ It was concluded that Mo should occupy the $8i$ site, which was supported by most of the experimental results.^{12,22} Here our results agree in principle that Mo occupies the $8i$ site, however, the refinement irrefutably showed that Mo also substitutes a small fraction of Fe atoms on the $8f$ site. Since the shortest Fe - Fe distance is between the $8f$ and $8f$ sites (2.385 Å at 10 K, Table IV), partial substitution of Fe by Mo on this site is favorable in view of the structure stabilization.

The magnetic moment was refined last, by fixing all the crystallographic parameters. The 2θ range used for moment refinement was only up to 100° because of the rapid fall off in the magnetic form factor. The initial values were taken from data obtained by magnetization measurement. The Y moment was fixed to be 0. According to spin-polarized band-structure calculations, V and Cr have magnetic moments of about $1\mu_B$ coupled antiparallel to Fe moments in $\text{YFe}_{10}\text{V}_2$ and $\text{YFe}_{10}\text{Cr}_2$.²³ Since Mo is in the same column as Cr in the Periodic Table, Mo could have moments of the same nature. We also got better reliability factors when assigned a moment of $-1\mu_B$ instead of $0\mu_B$ on Mo sites. Thus the Mo moment was assumed to be $-1\mu_B$ at 10 K and not refined. For the RT data, linear constraints of equal moment on all the Fe sites were imposed. In this case, both Y and Mo

TABLE II. Refined parameters of YFe_{11}Mo and $\text{YFe}_{11}\text{MoN}_{1.0}$ at 10 K. Symbols have the same meaning and units as in Table I.

YFe_{11}Mo : $R_1=3.74\%$; $R_F=3.14\%$						
Site	Atom	n	x	y	z	m
$2a$	Y	1.0	0	0	0	0
$8i$	Fe	0.80(2)	0.3587(7)	0	0	2.36(55)
	Mo	0.20(2)	0.3587(7)	0	0	-1.0
$8j$	Fe	1.00(2)	0.2769(7)	0.5	0	2.42(64)
$8f$	Fe	0.95(2)	0.25	0.25	0.25	2.15(45)
	Mo	0.05(2)	0.25	0.25	0.25	-1.0
$\text{YFe}_{11}\text{MoN}_{1.0}$: $R_1=3.47\%$; $R_F=2.77\%$						
$2a$	Y	1.0	0	0	0	0
$8i$	Fe	0.80(2)	0.3609(9)	0	0	2.43(44)
	Mo	0.20(2)	0.3609(9)	0	0	-1.0
$8j$	Fe	1.00(2)	0.2761(8)	0.5	0	2.32(92)
$8f$	Fe	0.95(2)	0.25	0.25	0.25	2.38(33)
	Mo	0.05(2)	0.25	0.25	0.25	-1.0
$2b$	N	0.94(8)	0	0	0.5	0

TABLE III. Refined parameters of YFe_9Mo_3 and $\text{YFe}_9\text{Mo}_3\text{N}_{1.0}$ at room temperature. Symbols have the same meaning and units as in Table I.

YFe_9Mo_3 : $R_1=3.93\%$; $R_F=3.12\%$						
Site	Atom	n	x	y	z	B
$2a$	Y	1.0	0	0	0	0.76
$8i$	Fe	0.35(2)	0.358(1)	0	0	0.35
	Mo	0.65(2)	0.358(1)	0	0	0.52
$8j$	Fe	1.00(2)	0.282(1)	0.5	0	0.35
$8f$	Fe	0.90(2)	0.25	0.25	0.25	0.35
	Mo	0.10(2)	0.25	0.25	0.25	0.52
$\text{YFe}_9\text{Mo}_3\text{N}_{1.0}$: $R_1=3.90\%$; $R_F=3.32\%$						
$2a$	Y	1.0	0	0	0	1.29
$8i$	Fe	0.35(2)	0.360(1)	0	0	0.46
	Mo	0.65(2)	0.360(1)	0	0	0.46
$8j$	Fe	1.00(2)	0.279(1)	0.5	0	0.46
$8f$	Fe	0.90(2)	0.25	0.25	0.25	0.46
	Mo	0.10(2)	0.25	0.25	0.25	0.46
$2b$	N	0.94(7)	0	0	0.5	0.20

TABLE IV. Interatomic distance (\AA) of YFe_{11}Mo and $\text{YFe}_{11}\text{MoN}_{1.0}$ at 10 K, YFe_9Mo_3 and $\text{YFe}_9\text{Mo}_3\text{N}_{1.0}$ at room temperature. $2a$ is the site occupied by Y; $8i$ is occupied by both Fe and Mo; $8j$ is occupied by Fe and $2b$ is the N site.

Site	YFe_{11}Mo	$\text{YFe}_{11}\text{MoN}_{1.0}$	YFe_9Mo_3	$\text{YFe}_9\text{Mo}_3\text{N}_{1.0}$
$2a-2a \times 1$	4.770	4.790	4.814	4.827
$2a-8i \times 4$	3.052	3.111	3.069	3.133
$2a-8j \times 8$	3.048	3.076	3.047	3.086
$2a-8f \times 8$	3.236	3.274	3.261	3.305
$2a-2b \times 2$		2.395		2.414
$8i-2a \times 1$	3.052	3.111	3.069	3.133
$8i-8i \times 1$	2.405	2.398	2.434	2.437
$8i-8i \times 4$	2.929	2.934	2.959	2.966
$8i-8j \times 2$	2.645	2.665	2.706	2.716
$8i-8j \times 2$	2.649	2.670	2.690	2.700
$8i-8f \times 4$	2.608	2.644	2.626	2.666
$8i-2b \times 2$		3.926		3.955
$8j-2a \times 2$	3.048	3.076	3.047	3.086
$8j-8i \times 2$	2.645	2.665	2.706	2.716
$8j-8i \times 2$	2.649	2.670	2.690	2.700
$8j-8j \times 2$	2.685	2.730	2.643	2.720
$8j-8f \times 4$	2.450	2.476	2.473	2.501
$8j-2b \times 1$		1.930		1.923
$8f-2a \times 1$	3.236	3.274	3.261	3.305
$8f-8i \times 4$	2.608	2.644	2.626	2.666
$8f-8i \times 4$	2.450	2.476	2.473	2.501
$8f-8f \times 2$	2.385	2.395	2.407	2.414
$2b-2a \times 2$		2.395		2.414
$2b-8i \times 8$		3.926		3.955
$2b-8j \times 4$		1.930		1.923
$2b-8f \times 8$		3.274		3.305

moments were assumed to be zero.

We must mention here that the *statistical* errors on the magnetic moment are quite large, as shown in the tables. Due to the difficulties in magnetic-moment determination by the neutron-powder-diffraction method, the absolute value of moment on each crystallographic site may not be very accurate, but definite conclusions can nevertheless be drawn, especially the influence of the interstitial N

atom on the moment at different Fe sites, which will be discussed in the next section.

Diffraction patterns of YFe_{11}Mo were fitted with a single phase only. In Fig. 2, a small peak(s) around $2\theta=53^\circ$, which does not belong to the ThMn_{12} structure, can be observed. This peak is possibly due to a very small amount of Fe impurity phase in the sample since the strongest peak of $\alpha\text{-Fe}$ appears at $2\theta=53.4^\circ$. The other possibility is coming from the sample holder, where a little piece of Al is used at the bottom. The Al (200) reflection also appears at $2\theta=53.5^\circ$.

B. $\text{YFe}_{11}\text{MoN}_{1.0}$

Refinement of diffraction patterns of YFe_{11}Mo nitride is based on the results of YFe_{11}Mo . As shown already by previous works,^{12,22,24} the nitrides retain the crystallographic symmetry of the host compounds. As nitrogenation was conducted at relatively low temperature (773 K), it is not possible to interfere Mo occupancy by nitrogenation. Thus the occupation factors of Mo were not refined and kept to be the same as in the host compound. Nitrogen atoms were assigned at the $2b$ site, obviously this being the only possible site with enough space for N atoms in the structure. The occupation factor of N on the $2b$ site was refined. The diffraction pattern of $\text{YFe}_{11}\text{MoN}_{1.0}$ at 10 K is shown in Fig. 3. Refinement results are compared with those of its host compound in Tables I and II for data at RT and 10 K, respectively. Bond lengths at 10 K are listed together with those of YFe_{11}Mo in Table IV. Lattice parameters are in Table V.

Comparing Fig. 2 with Fig. 3, it can be seen clearly that the impurity peak(s) at about $2\theta=53^\circ$ is stronger in the nitride, although part of the intensity contributed from the (330) peak, which belongs to the 1:12 phase and shifts to nearly the same position of the main peak of Fe after nitrogenation. In the nitrogenation process, it is inevitable that a small amount of impurity phases such as iron and rare earth nitride are formed. The nitrogenation condition has to be carefully controlled in order to reduce the amount of impurities as much as possible.

The refinements of the diffraction patterns of $\text{YFe}_{11}\text{MoN}_{1.0}$ were performed in three different ways: (1) assuming single phase and using the whole intensity data; (2) assuming single phase but excluding data of the im-

TABLE V. Lattice parameters and average magnetic moment on the Fe site. m^* is the data taken from Ref. 14, which were obtained by magnetization measurements.

	YFe_{11}Mo	$\text{YFe}_{11}\text{MoN}_{1.0}$	YFe_{11}Mo	$\text{YFe}_{11}\text{MoN}_{1.0}$	YFe_9Mo_3	$\text{YFe}_9\text{Mo}_3\text{N}_{1.0}$
$T(\text{K})$	300	300	10	10	300	300
$a(\text{\AA})$	8.512 08(8)	8.629 25(9)	8.509 67(6)	8.620 12(9)	8.572 0(1)	8.702 2(1)
$c(\text{\AA})$	4.777 79(5)	4.796 63(6)	4.769 81(5)	4.789 47(7)	4.813 85(9)	4.827 34(9)
$V(\text{\AA}^3)$	346.18	357.18	345.40	355.89	353.72	365.57
$\Delta a/a(\%)$		1.376 5		1.297 9		1.518 9
$\Delta c/c(\%)$		0.394 3		0.412 2		0.280 2
$\Delta V/V(\%)$		3.177		3.036		3.350
$\Delta V/N(\text{\AA}^3)$		5.85		5.58		6.30
$m(\mu_B)$	1.50	1.65	2.22	2.28		
$m^*(\mu_B)$	1.51	1.99	2.15	2.25		0.81

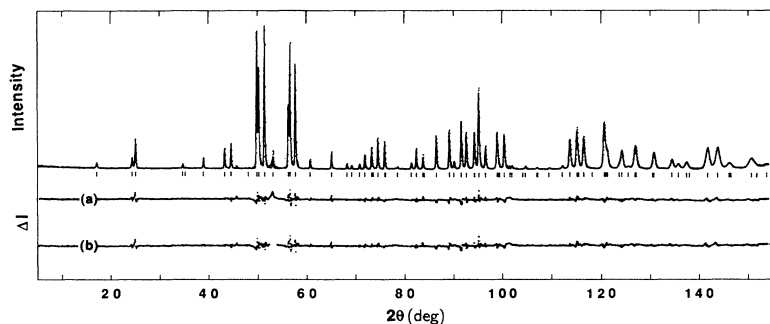


FIG. 3. Neutron-powder-diffraction pattern of $\text{YFe}_{11}\text{MoN}_{1.0}$ at 10 K. The dots and line correspond to the observed and the calculated patterns, respectively. The lower part is the difference pattern (observed-calculated). (a) The whole intensity data were used and (b) data of the impurity peak 2θ range from 52.5° to 54° were deleted. The calculated peak positions are indicated by the bars.

purity peak 2θ region from 52.5° to 54° ; and (3) assuming two phases (1:12 phase and α -Fe phase) and using the whole data. However, the refined parameters of the 1:12 phase were not affected at all within the statistical errors by the three different methods. By using the single-phase model, when the impurity peak range was excluded, the R factors were improved. When using the two-phase model, we had the difficulty of getting acceptable R factors ($< 10\%$) on the impurity phase, perhaps because the second phase is not well-crystallized α -Fe. The lattice parameter of the impurity phase was found to be slightly larger than that of α -Fe and the shape of the peak was quite broad. It could be iron with very fine particle size and a small amount of dissolved nitrogen. It should be noted here that data listed in Tables I and II are the refinement results obtained by using the single-phase model but excluding data in the 2θ range from 52.5° to 54° . Both difference patterns obtained by using methods (1) and (2) are plotted in Fig. 3, as indicated by (a) and (b) in the figure.

The nitrogen occupation factor on the $2b$ site is very close to 1, suggesting the nitrogenation of the 1:12 phase is complete and homogeneous. The nitrogen content is also comparable with the value 1.0 ± 0.1 determined by sample mass increase. The fully nitrogenated 1:12 phase gives sharp diffraction peaks and allows us to get reliable information on the nitride.

N insertion results in an expanded lattice cell with expansion mainly along the a axis (Table V). The N-occupied $2b$ site is at the center of an octahedron formed by 4-Fe($8j$) atoms and 2-Y($2a$) atoms. It is equivalent to the $9e$ or $6h$ site in the 2:17 structure. The neighborhood of the rare-earth site is most seriously modified. Two additional N atoms, which are located along the c axis, became nearest neighbors of the rare-earth atoms, while the Fe (or Mo) nearest neighbors ($8i$ and $8j$), which are locat-

ed in the basal plane, remained at about the same distance as in the host alloy (Table IV). Such drastic change of the rare-earth environment must have a large influence on the magnetic anisotropy properties, as has been observed experimentally. The room-temperature easy magnetization direction of $\text{SmFe}_{11}\text{Ti}$ was changed from parallel to c axis to perpendicular to c axis after nitrogenation.²⁵ It has been proposed that the crystal electric-field parameter A_{20} at the rare-earth site is mainly due to the aspherical charge density distribution of the valence electrons of the R atoms.²⁶ As the difference of electronegativity between N and R is large, two N nearest neighbors of the rare-earth along the c axis could induce a considerable valence charge redistribution of the R atoms. Furthermore, the rare-earth valence charge density should be stabilized close to the c axis, because of the much stronger electronegativity of N atoms. As a result, A_{20} changes its sign from negative to positive upon nitrogenation.²⁷

Here it is worthwhile to compare the R -N bond length in the 1:12 nitrides with that in the 2:17 nitrides. The Y-Fe bond length, deduced from the neutron-diffraction data by Ibberson *et al.*,²⁸ is 2.49 \AA in $\text{Y}_2\text{Fe}_{16.5}\text{N}_{2.9}$, while that in $\text{YFe}_{11}\text{MoN}_{1.0}$ is only 2.398 \AA . This shorter bond length is the main reason for the much larger effects of nitrogenation on the rare-earth crystal-field interactions in the 1:12 structure than in the 2:17 structure. The nitrogen-induced shift in A_{20} per neighboring nitrogen atom was estimated by Li and Cadogan using the bonding-charge model, which gave $+200 \text{ ka}_0^{-2}$ for $\text{NdFe}_{11}\text{TiN}_{1-\delta}$ (Ref. 29) and -63 ka_0^{-2} for $\text{Sm}_2\text{Fe}_{17}\text{N}_{3-\delta}$.³⁰

Procedure and considerations on moments refinement are the same as for YFe_{11}Mo . Comparing the data at 10 K of $\text{YFe}_{11}\text{MoN}_{1.0}$ with its host compound YFe_{11}Mo , it

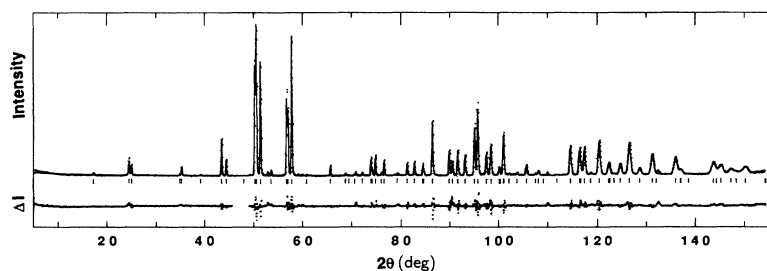


FIG. 4. Neutron-powder-diffraction pattern of YFe_9Mo_3 at RT. The dots and line correspond to the observed and the calculated patterns, respectively. The lower part is the difference pattern (observed-calculated). The calculated peak positions are indicated by the bars.

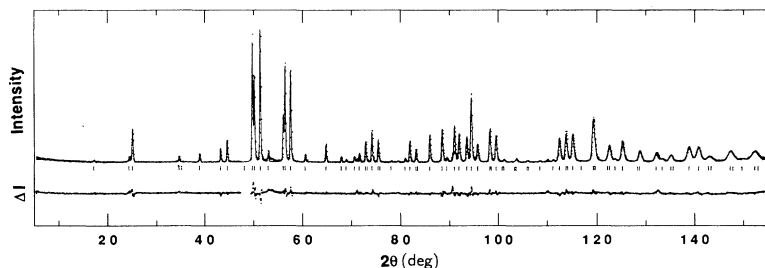


FIG. 5. Neutron-powder-diffraction pattern of $\text{YFe}_9\text{Mo}_3\text{N}_{1.0}$ at RT. The dots and line correspond to the observed and the calculated patterns, respectively. The lower part is the difference pattern (observed-calculated). The calculated peak positions are indicated by the bars.

is clear that after nitrogenation Fe moments on the $8i$ and $8f$ sites increased and that on the $8j$ site decreased. This result is in agreement with most of the band-structure calculations.^{31–33} The effect of interstitial N on Fe moment is twofold; enhancing the moment by narrowing the $3d$ bands as a result of the volume expansion and reducing the moment by hybridization of N- $2p$ and Fe- $3d$ orbitals. The latter one is dominant for the $8j$ site since it is the nearest neighbor of N located on the $2b$ site (Table IV). The net effect of nitrogenation leads to an increase of the average moment, but only slightly.

The average moment is listed and compared with the experimental data in Table V. The disagreement of the RT data of $\text{YFe}_{11}\text{MoN}_{1.0}$ is another indication of the existence of an iron impurity phase. The impurity phase has stronger influence on the magnetic moment at RT than at 10 K, because of its much higher Curie temperature. However, this disagreement in moment cannot be attributed to the iron impurity phase entirely; errors in both magnetization measurements and neutron-diffraction data refinements should also be taken into account. The average moments at 10 K are also comparable with those obtained by band-structure calculation on $\text{YFe}_{12-x}\text{Mo}_x$ and its nitride.³⁴

C. YFe_9Mo_3 and $\text{YFe}_9\text{Mo}_3\text{N}_{1.0}$

Diffraction patterns and the fits for YFe_9Mo_3 and $\text{YFe}_9\text{Mo}_3\text{N}_{1.0}$ are shown in Figs. 4 and 5, respectively. Refined parameters, bond lengths, and lattice parameters are displayed in Tables III, IV, and V, respectively. Since the magnetic ordering temperatures of both YFe_9Mo_3 and its nitride are quite low (138 K and 342 K),¹⁴ magnetic contributions to the diffraction intensity were not included during the refinements. In the host compounds, apart from a small amount of iron impurity phase, there are other impurities which manifest their existence in the 2θ range from 47° to 49° . There could be some kind of compounds between Fe and Mo. Luckily there are no diffraction peaks from the 1:12 phase in this region, hence intensity data in this range were deleted during the refinement for both the host and the nitride. Similar to the case of iron impurity in YFe_{11}Mo and $\text{YFe}_{11}\text{MoN}_{1.0}$, excluding this range has no influence on the refinement results of the 1:12 phase, but only the R factors were improved. The iron impurity region was not excluded during the fitting.

For YFe_9Mo_3 , Mo occupancies were carefully refined. Final results gave 65% occupation of the $8i$ site, 10% of the $8f$ site and no occupation on the $8j$ site. Keeping the

same site occupancy by Mo, the N content in $\text{YFe}_9\text{Mo}_3\text{N}_{1.0}$ was investigated. Refinement yields a value of 0.94 ± 0.07 N atoms per formula unit. While this value indicates that the 1:12 phase was nearly ideally nitrogenated, it is much lower than the number deduced from mass increase upon nitrogenation, which gave 1.4 ± 0.1 . We attribute this difference partially to the Fe-Mo impurities existing already in the host YFe_9Mo_3 compound. The Fe-Mo compound could also absorb a certain amount of nitrogen atoms.

IV. CONCLUSIONS

Homogeneous and completely nitrogenated YFe_{11}Mo and YFe_9Mo_3 were successfully made. Conclusive results as regarding to the crystallographic parameters of both the host compounds and their nitrides were obtained by analyzing the neutron-powder-diffraction patterns. Mo occupies mainly the $8i$ site, while it also substitutes a small fraction of Fe on the $8f$ site. Nitrogen atoms located at the $2b$ interstitial sites, which is equivalent to the $6h$ or $9e$ site in the 2:17 structure. Upon nitrogenation, the crystallographic symmetry of the host is retained, but the lattice cell is expanded by more than 3%. Two nitrogen atoms become the nearest neighbors of the rare-earth site, which is responsible for the radical changes of the magnetocrystalline anisotropy properties. Nitrogenation also modifies the Fe magnetic moment, particularly the individual moment on each crystallographic site, resulting in an enhanced moment on the $8i$ and $8f$ sites and a reduced moment on the $8j$ site, which is the nearest neighbor of N $2b$ site. The average moment, which is hardly influenced by nitrogenation, is comparable with data obtained by the magnetization measurement.

ACKNOWLEDGMENTS

H.S. was supported by the Japan Society for the Promotion of Science (JSPS). The financial support from the International Joint Research Project of the NEDO Japan is gratefully acknowledged. We thank Y. Shimojyo for his technical assistance in the diffraction experiments and the people working at the Department of Research Reactor of Japan Atomic Energy Research Institute for their supports at JRR-3M. We benefited greatly from enlightened discussions with Professor T. Kajitani of Tohoku University. At the very early stage of sample preparation, we received generous help from Y. Kawado and T. Shimizu of Mazada Co. Ltd., which was very much appreciated.

- ¹J. M. D. Coey and Hong Sun, *J. Magn. Magn. Mater.* **87**, L251 (1990).
- ²X. D. Zhang, Q. Pan, S. L. Ge, Y. C. Yang, J. L. Yang, Y. F. Ding, B. S. Zhang, C. T. Ye, and L. Jin, *Solid State Commun.* **83**, 231 (1992).
- ³F. M. Yang, Q. A. Li, Y. Lu, N. Tang, O. Tegus, M. J. Yu, R. W. Zhao, B. G. Shen, and L. Y. Yang, *J. Magn. Magn. Mater.* **14**, 255 (1992).
- ⁴J. M. D. Coey and D. P. F. Hurley, *J. Magn. Magn. Mater.* **104-107**, 1098 (1992).
- ⁵W. E. Wallace and M. Q. Huang, *IEEE Trans. Magn.* **MAG-28**, 2312 (1992).
- ⁶J. M. D. Coey, *Physica Scripta* **T39**, 21 (1991).
- ⁷Hong Sun, J. M. D. Coey, Y. Otani, and D. P. F. Hurley, *J. Phys.: Condens. Matter* **2**, 6465 (1990).
- ⁸D. P. F. Hurley and J. M. D. Coey, *J. Phys.: Condens. Matter* **4**, 5573 (1992).
- ⁹M. Katter, J. Wecker, C. Kuhrt, L. Schultz, and R. Grössinger, *J. Magn. Magn. Mater.* **117**, 419 (1992).
- ¹⁰H. Fujii, K. Yamamoto, K. Tatami, and M. Akayama, in *Proceedings of the 2nd International Symposium on Physics of Magn. Mater., Beijing, China* (Academic, New York, 1992), p. 624.
- ¹¹C. Kuhrt, K. O'Donnell, M. Katter, J. Wecker, K. Schnitzke and L. Schultz, *Appl. Phys. Lett.* **60**, 3316 (1992).
- ¹²W. B. Yellon and G. C. Hadjipanayis, *IEEE Trans. Magn.* **MAG-28**, 2316 (1992).
- ¹³O. Isnard, S. Miraglia, J. L. Soubeyroux, D. Fruchart, and J. Pannetier, *Phys. Rev. B* **45**, 2920 (1992).
- ¹⁴Hong Sun, M. Akayama, K. Tatami, and H. Fujii, *Physica B* **183**, 33 (1993).
- ¹⁵H. Fujii, K. Tatami, M. Akayama, and K. Yamamoto, in *Proceedings of the Sixth International Conference on Ferrites (ICF6)*, edited by T. Yamaguchi and M. Abe (The Japan Society of Powder and Powder Metallurgy, Tokyo, 1992), p. 1081.
- ¹⁶O. Isnard, S. Miraglia, J. L. Soubeyroux, and D. Fruchart, *J. Alloys Compounds* **190**, 129 (1992).
- ¹⁷Y. Morii, K. Fuchizaki, S. Funahashi, N. Minakawa, Y. Shimojyo, and A. Ishida, in *Proceedings of the 4th International Symposium on Advanced Nuclear Energy Research, 1992, Mito, Japan*, edited by T. Kondo (Japan Atomic Energy Research Institute, Ibaraki, 1992) p. 280.
- ¹⁸F. Izumi, in *The Rietveld Method*, edited by R. A. Young (Oxford University Press, Oxford, 1993), Chap. 13.
- ¹⁹V. F. Sears, in *Neutron Scattering (Part A), Methods of Experimental Physics*, edited by K. Sköld and D. L. Price (Academic, New York, NY, 1986), p. 521.
- ²⁰G. E. Bacon, *Neutron Diffraction* (Clarendon, Oxford, 1975), Chap. 7.
- ²¹D. B. de Mooij and K. H. J. Buschow, *J. Less-Common Met.* **136**, 207 (1988).
- ²²V. Psychairs, M. Anagnostou, C. Christides, and D. Niarchos, *J. Appl. Phys.* **70**, 6122 (1991).
- ²³S. S. Jaswal, Y. G. Ren, and D. J. Sellmyer, *J. Appl. Phys.* **67**, 4564 (1990).
- ²⁴Y. C. Yang, X. D. Zhang, L. S. Kong, Q. Pan, S. L. Ge, J. L. Yang, Y. F. Ding, B. S. Zhang, C. T. Ye, and L. Jin, *Solid State Commun.* **78**, 313 (1991).
- ²⁵J. M. D. Coey, Y. Otani, Hong Sun, and D. P. F. Hurley, *J. Magn. Soc. Jpn.* **15**, 769 (1991).
- ²⁶X. F. Zhong and W. Y. Ching, *Phys. Rev. B* **39**, 12018 (1989).
- ²⁷R. Coehoorn, *J. Magn. Magn. Mater.* **99**, 55 (1991).
- ²⁸R. M. Ibberson, O. Moze, T. H. Jacobs, and K. H. J. Buschow, *J. Phys.: Condens. Matter* **3**, 1219 (1991).
- ²⁹H. S. Li and J. M. Cadogan, *J. Magn. Magn. Mater.* **109**, L153 (1992).
- ³⁰H. S. Li and J. M. Cadogan, *Solid State Commun.* **80**, 905 (1991).
- ³¹Y. P. Li and J. M. D. Coey, *Solid State Commun.* **81**, 447 (1992).
- ³²S. Asano, S. Ishida, and S. Fujii, *Physica B* **190**, 155 (1993).
- ³³A. Sakuma, *J. Phys. Soc. Jpn.* **61**, 4119 (1992).
- ³⁴S. Ishida and S. Asano (private communications).